COMMUNICATION

Pt-TiO_2 catalysts for glycerol photoreforming: impact of surface hydration of anatase, brookite and rutile polymorphs

Received 00th January 20xx,
Accepted 00th January 20xx

DOI: 10.1039/x0xx00000x

Claudio Maria Pecoraro,[a] Lorenzo Mino,*[b] Elizaveta Kozyr,[b] Leonardo Palmisano,[a] Francesco di Franco,[a] Vittorio Loddo,[a] Monica Santamaria,[a] Marianna Bellardita*[a]

The H_2 production from glycerol photoreforming increases in the order Pt-Rutile < Pt-P25 ≈ Pt-Anatase < Pt-Brookite with a different distribution of the reaction intermediates. The highest brookite activity is attributed to its ability to adsorb water and to the different distribution of Pt active sites present at its surface.

In recent years, great attention has been paid in the field of heterogeneous photocatalysis to photo-reforming reactions, i.e. the partial oxidation of organic compounds, generally biomass derivatives, to chemicals with the contemporary production of H_2,[1] since the direct splitting of water is a very difficult process to carry out both from a thermodynamic and kinetic point of view. In this way an efficient utilization of both photoproduced holes for organics partial oxidation and electrons for H^+ reduction is possible. Among the different semiconductors, TiO_2 is the most used photocatalyst because of its easy availability, low cost, non-toxicity, chemical stability in the reaction media and high catalytic activity.[2] TiO_2 displays different polymorphs and three are those more used as photocatalysts: anatase, brookite, and rutile.[3] Generally, the polymorphs have different surface, chemical and electronic properties that determine the photocatalytic activity,[4] although also the specific substrate-catalyst interaction must always be considered.[5] Moreover, previous works demonstrated that activity of the same TiO_2 phase is extremely variable depending on the particle sizes, specific surface area, porosity, exposed crystal facets, surface hydroxylation degree and amount of hydroxyl radicals produced under irradiation.[6] In fact, in some specific cases, rutile and brookite are reported to be more active than anatase towards H_2 production[7] and the binary or ternary mixtures are generally more active than the single phases because of the favoured spatial separation of the photo-generated charges in the coupled systems.[8] Moreover, brookite and rutile are generally less active than anatase in pollutant degradation reactions but are effective in partial oxidation reactions.[3a, 9]

In this work the activity of anatase, rutile and brookite TiO_2 polymorphs, functionalized with Pt as co-catalyst, has been compared towards the photoreforming of glycerol,[10] used as model biomass compound, under both UV and simulated solar light irradiation. The worldwide used commercial TiO_2 P25 was used for the sake of comparison. FT-IR spectroscopy was employed to assess the water adsorption properties and to probe, by CO adsorption, the Pt active sites to correlate the photocatalytic activity with the catalyst surface properties.

The details of the synthesis, characterization and photocatalysis tests are reported in the Supplementary Information.

The X-ray diffraction patterns of the synthesized materials (Figure S1A) show the main characteristic peaks of anatase (2θ = 25.5°, 38.0°, 48.0°, 54.5°), rutile (2θ = 27.5°, 36.5°, 41°, 54.1°, 56.5°) and brookite (2θ = 25.34°, 25.69◦, 30.81°), confirming the presence of the three pure TiO_2 phases in the home-made samples and the coexistence of anatase and rutile in P25. The presence of the photodeposited Pt was not noticed due to its low amount. The peaks of Pt-P25 and Pt-Anatase are more intense and narrower than those of Pt-Brookite and Pt-Rutile, indicating a greater crystallinity and a larger crystallite size (Table 1) in accordance with the higher temperature at which they were prepared. Raman spectra (Figure S1B) confirm the XRD results and, in particular, the purity of Pt-Brookite. In fact, while the main XRD peaks of brookite and anatase are practically coincident, the Raman bands of brookite are distinct from those of anatase.[11] The specific surface area (SSA) of Pt-Anatase is very similar to that of Pt-P25, being 48 $m^2 \cdot g^{-1}$ and 50 $m^2 \cdot g^{-1}$, respectively, while Pt-Brookite and Pt-Rutile display higher values (Table 1).

[a] *Engineering Department, University of Palermo, Viale delle Scienze Ed. 6, Palermo, 90128, Italy. E-mail: marianna.bellardita@unipa.it*
[b] *Department of Chemistry and Interdepartmental Centre NIS, University of Torino, Via Giuria 7, 10125 Torino, Italy. E-mail: lorenzo.mino@unito.it*

Electronic Supplementary Information (ESI) available: [details of any supplementary information available should be included here]. See DOI: 10.1039/x0xx00000x

Table 1. TiO_2 phase (A=Anatase, R=Rutile, B= Brookite), crystallite size (Φ), specific surface area (SSA) and band-gap (E_g) for the different samples.

Sample	Crystalline phase	S.S.A ($m^2 g^{-1}$)	Φ (nm)	E_g (eV)
Pt-P25	A, R	50	27 (A) 31 (R)	3.10
Pt-Anatase	A	48	22	3.26
Pt-Brookite	B	83	7	3.34
Pt-Rutile	R	85	4	3.02

The diffuse reflectance UV-Vis spectra of the different TiO_2 samples are reported in Figure S2. As visible in Table 1, rutile shows the smallest band gap values, while the transition is shifted to higher energies for anatase and brookite, as expected from literature results.[12] The commercial P25 exhibits an onset in the absorption in the UV region (λ ≈ 360 nm) typical of the anatase/rutile mixture. The presence of platinum does not change the band gap transition but only increases the visible light absorption.[7b]

SEM images (Figure S3) reveal that the photocatalysts are formed of aggregates of irregular spherical particles with dimensions in the nanometric scale. Pt particles are not distinguishable due to their small amount and uniform distribution on the TiO_2 surface.

In Table 2 the results related to the photoreforming of glycerol after 4 h of irradiation under both UV and solar light irradiation are presented in terms of glycerol conversion, selectivity towards the main reaction intermediates (1,3-dihydroxyacetone and glyceraldehyde) and concentration of CO_2 and H_2 in the gas phase accumulated in the headspace of the reactor.

Table 2. Photocatalytic results obtained after 4 h of UV or simulated solar light irradiation. X = glycerol conversion, S = selectivity. DHA = 1,3-dihydroxyacetone, GA = glyceraldehyde

Sample	X	S_{DHA} [%]	S_{GA} [%]	CO_2 [mM]	H_2 [mM]	H_2/CO_2
UV irradiation						
Pt-P25	23	6.4	9.8	0.09	3.0	33.3
Pt-Anatase	14	14.4	22.5	0.11	3.0	27.3
Pt-Brookite	26	6.8	8.1	0.23	9.3	40.4
Pt-Rutile	13	10.6	21.6	0.06	1.2	20
Simulated solar light irradiation						
Pt-P25	20	8.8	11.0	0.10	3.1	31
Pt-Brookite	21	9.1	10.0	0.18	5.4	30

All photocatalysts give rise to the same partial oxidation compounds, indicating a similar reaction pathway. However, we can observe a different degree of conversion, selectivity towards the intermediates and H_2 production. Under UV irradiation in the presence of Pt-P25, glycerol reaches a conversion of 23% with a selectivity of 6.4% and 9.8% towards DHA and GA, respectively and a H_2 concentration of 3.0 mM. Among the home prepared catalysts, Pt-Anatase and especially Pt-Rutile display a lower glycerol conversion and H_2 formation. Pt-Brookite shows almost the same activity as P25 regarding the partial oxidation of glycerol (23% conversion vs 26%) but was more active towards the H_2 production being the quantity obtained 3.1 times greater. Also, under simulated solar light irradiation Pt-Brookite is more performant that Pt-P25. As well-known from literature, during a photoreforming process, the H_2 comes from both water splitting and sacrificial agent (glycerol in our case) dehydrogenation (Scheme 1).[1b, 1d] Evaluating the H_2/CO_2 ratio we can note that the highest value is obtained with broookite (Table 2). Moreover, by comparing Pt-Brookite and Pt-P25 a higher mineralization degree was found for the first photocatalyst. This finding suggests a greater contribution in the H_2 production of the water splitting with respect to glycerol reforming under UV irradiation in the presence of brookite. In fact, as the mineralization of glycerol gives rise to H_2O and CO_2, the higher H_2/CO_2 ratio can be due to a more significant contribution of water splitting. Under solar light irradiation, instead, virtually the same ratio was obtained with Pt-P25 and Pt-Brookite. This could be an indirect confirmation that the water splitting requires more energy than photoreforming, that is, the addition of a sacrificial agent makes the activation energy lower for the formation of hydrogen, in accordance with the literature.[1b]

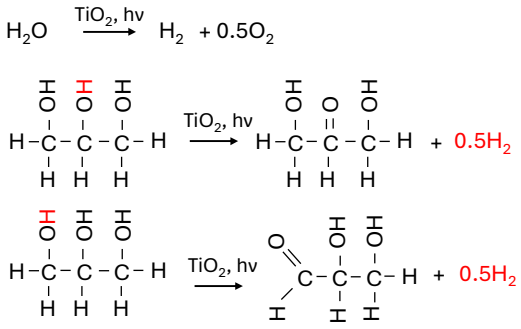

Scheme 1. Main products from photocatalytic glycerol reforming.

To understand which can be the impact of the catalyst surface properties on the observed photocatalytic activity, we performed an *in situ* FT-IR study. As first step, we performed a systematic investigation of the adsorption of molecular water by dosing controlled pressures of water on the different samples. Figure 1 reports the spectral region typical of the water bending mode which is particularly suitable to compare the amount of H_2O adsorbed by the different polymorphs. We can note that at maximum water coverage (blue curves in Figure 1) for all the materials the position of the δ(H_2O) band is significantly blueshifted with respect to the bending mode of water in gas phase which lies at 1595 cm^{-1}.[13] This behaviour is associated with H_2O molecules acting as H-bond donors [14] and it is particularly evident for Pt-Anatase and Pt-P25, both showing a maximum at ca. 1635 cm^{-1}, while is more limited for Pt-Rutile (maximum at 1627 cm^{-1}) and for Pt-Brookite (maximum at 1622 cm^{-1}). Upon water outgassing, the bands redshift owing to the fading out of the water-water interactions moving from multilayers of adsorbed H_2O to the monolayer. [14a] The final band position after 15 minutes of outgassing is 1625 cm^{-1} for Pt-Anatase, 1621 cm^{-1} for Pt-P25, 1618 cm^{-1} for Pt-

Rutile and 1611 cm^{-1} for Pt-Brookite. Concerning the intensity of the bands, we can see that the $\delta(H_2O)$ signals follow the order Pt-Brookite >> Pt-P25 ≈ Pt-Anatase > Pt-Rutile, highlighting a remarkably higher hydrophilicity for the brookite-based sample. These findings are in agreement with previous results obtained by contact angle measurements on TiO_2 anatase, rutile and brookite films, which revealed that the brookite films were the most hydrophilic ones.[15]

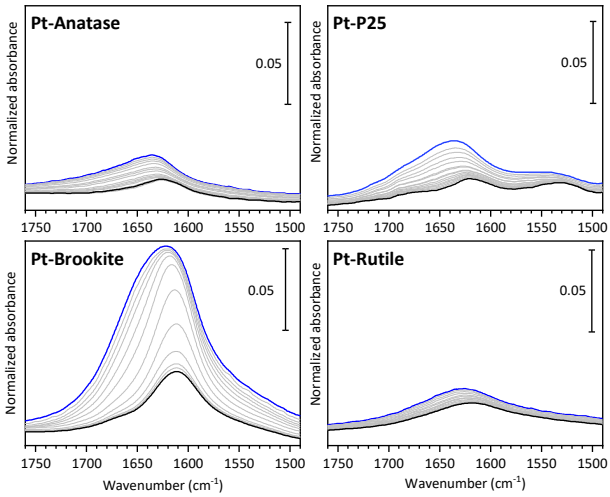

Figure 1. FT-IR spectra of the different materials in contact with H_2O at 15 mbar (blue curve) and progressive decreasing of the water coverage till outgassing for 15 minutes at beam temperature (black curve).

To investigate the properties of the surface active sites in the different samples, we employed carbon monoxide, which is a versatile probe molecule, able to interact with both Ti and Pt centers. Before performing CO adsorption experiments, the surface of the materials must be "cleaned" from organic contaminants coming from the synthesis and adsorbed water molecules by outgassing at 673 K. The samples were then treated in H_2 at 423 K to reduce the Pt nanoparticles, mimicking the reducing conditions present during the photocatalytic reactions (see the Supplementary Information for more details). Upon CO adsorption, we can observe in all samples a band around 2180 cm^{-1} (Figure 2), which can be ascribed to the interaction of CO with Ti^{4+} cations. This spectral feature is particularly sharp in Pt-P25, owing to the high regularity of the anatase {101} facets in this sample which is characterized by an excellent crystallinity.[16] These signals are in general quite weak owing to the low binding energy of CO on Ti^{4+} cations, which results in a low CO coverage of TiO_2 surfaces for room temperature adsorption.

Moving to the spectral features related to the interaction between CO and Pt sites, we can note the presence of a group of signals between 2135 and 2100 cm^{-1}, ascribed to $Pt^{\delta+}$-CO species,[17] which are more abundant in Pt-Rutile and Pt-Brookite. In previous studies these signals were associated to a significant metal-support interaction[18] and to a peculiar photocatalytic activity.[19] Furthermore, below 2100 cm^{-1} we can find the most intense bands due to the formation of linear carbonyls on metallic Pt.[20] In particular, the band at ca. 2080 cm^{-1}, which is dominant in Pt-P25 and Pt-Anatase, is ascribed to CO linearly adsorbed at terrace sites. Conversely, Pt-Rutile and Pt-Brookite show the most intense peak at lower wavenumbers, suggesting the presence of a higher fraction of edge and step sites. Indeed, it has been shown that a decrease in the coordination of the Pt^0 sites results in a redshift of the corresponding ν(CO) signal.[21] Therefore, we can also assign the tail located at ca. 2030 cm^{-1} to carbonyls on corners/kinks.[20] Finally, we can note that the main peak associated to metallic Pt sites is particularly narrow in the case of Pt-Brookite, highlighting a lower heterogeneity in the nanoparticle surface structure.

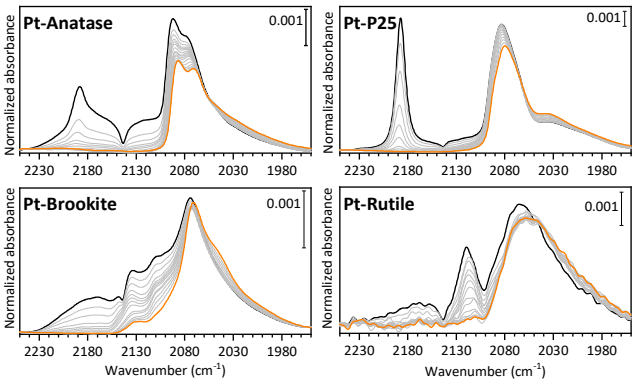

Figure 2. FT-IR spectra of the different materials, after activation at 673 K and reduction at 423 K, in contact with CO at 40 mbar (black curve) and progressive decreasing of the CO coverage till outgassing for 15 minutes at beam temperature (orange curve).

In summary our results show that the H_2 production from glycerol photoreforming and the intermediate products distribution are strongly dependent on the nature of the TiO_2 support. Brookite was the most active sample for H_2 production, and its amount decreases in the order Pt-Brookite > Pt-P25 ≈ Pt-Anatase > Pt-Rutile. This trend follows the hydrophilicity order of the different polymorphs since the measured intensity of the adsorbed water bending mode is Pt-Brookite >> Pt-P25 ≈ Pt-Anatase > Pt-Rutile. Employing IR spectroscopy of adsorbed CO we identified a different metal-support interaction for the investigated polymorphs, highlighting a lower concentration of $Pt^{\delta+}$ centers for Pt-P25 and Pt-Anatase. Moreover, the probe molecule showed a different distribution of low coordinated Pt^0 sites in the samples. We can thus conclude that the observed higher activity of the Pt-Brookite sample can be ascribed to its ability in adsorbing water, which is a key reactant to form hydrogen, and to the presence of a well-defined distribution of Pt^0 sites, preferentially located on edges and steps.

Conflicts of interest

There are no conflicts to declare.

Notes and references

1. (a) J. L. Ma, K. N. Liu, X. P. Yang, D. N. Jin, Y. C. Li, G. J. Jiao, J. H. Zhou and R. C. Sun, *ChemSusChem*, 2021, **14**, 4903-

4922; (b) U. Nwosu, A. G. Wang, B. Palma, H. Zhao, M. A. Khan, M. Kibria and J. G. Hu, *Renew. Sust. Energ. Rev.*, 2021, **148**, 111266; (c) M. Bellardita, V. Loddo and L. Palmisano, *Mini-Rev. Org. Chem.*, 2020, **17**, 884-901; (d) Y. Wang, L. Mino, F. Pellegrino, N. Homs and P. Ramirez de la Piscina, *Appl. Catal. B-Environ.*, 2022, **318**, 121783.

2. (a) K. Nakata and A. Fujishima, *J. Photochem. Photobiol. C-Photochem. Rev.*, 2012, **13**, 169-189; (b) H. R. Dong, G. M. Zeng, L. Tang, C. Z. Fan, C. Zhang, X. X. He and Y. He, *Water Res.*, 2015, **79**, 128-146.
3. (a) A. Di Paola, G. Cufalo, M. Addamo, M. Bellardita, R. Campostrini, M. Ischia, R. Ceccato and L. Palmisano, *Colloid Surf. A-Physicochem. Eng. Asp.*, 2008, **317**, 366-376; (b) M. L. Zhang, T. D. Chen and Y. J. Wang, *RSC Adv.*, 2017, **7**, 52755-52761.
4. (a) W. K. Li, X. Q. Gong, G. Lu and A. Selloni, *J. Phys. Chem. C*, 2008, **112**, 6594-6596; (b) L. Mino, G. Spoto, S. Bordiga and A. Zecchina, *J. Phys. Chem. C*, 2013, **117**, 11186-11196; (c) C. Günnemann, C. Haisch, M. Fleisch, J. Schneider, A. V. Emeline and D. W. Bahnemann, *ACS Catal.*, 2019, **9**, 1001-1012.
5. (a) M. Bellardita, M. Feilizadeh, R. Fiorenza, S. Scirè, L. Palmisano and V. Loddo, *Photochem. Photobiol. Sci.*, 2022, **21**, 2139-2151; (b) Z. Li, S. Cong and Y. M. Xu, *ACS Catal.*, 2014, **4**, 3273-3280.
6. (a) J. G. Li, T. Ishigaki and X. D. Sun, *J. Phys. Chem. C*, 2007, **111**, 4969-4976; (b) L. Mino, A. Zecchina, G. Martra, A. M. Rossi and G. Spoto, *Appl. Catal. B-Environ.*, 2016, **196**, 135-141; (c) F. Pellegrino, F. Sordello, L. Mino, C. Minero, V. D. Hodoroaba, G. Martra and V. Maurino, *ACS Catal.*, 2019, **9**, 6692-6697.
7. (a) E. Wierzbicka, M. Altomare, M. J. Wu, N. Liu, T. Yokosawa, D. Fehn, S. S. Qin, K. Meyer, T. Unruh, E. Spiecker, L. Palmisano, M. Bellardita, J. Will and P. Schmuki, *J. Mater. Chem. A*, 2021, **9**, 1168-1179; (b) M. Bellardita, E. I. García-López, G. Marcì and L. Palmisano, *Int. J. Hydrog. Energy*, 2016, **41**, 5934-5947.
8. (a) L. Q. Jing, S. D. Li, S. Song, L. P. Xue and H. G. Fu, *Sol. Energy Mater. Sol. Cells*, 2008, **92**, 1030-1036; (b) R. Kaplan, B. Erjavec, G. Drazic, J. Grdadolnik and A. Pintar, *Appl. Catal. B-Environ.*, 2016, **181**, 465-474.
9. M. Addamo, V. Augugliaro, M. Bellardita, A. Di Paola, V. Loddo, G. Palmisano, L. Palmisano and S. Yurdakal, *Catal. Lett.*, 2008, **126**, 58-62.
10. (a) S. Fujita, H. Kawamori, D. Honda, H. Yoshida and M. Arai, *Appl. Catal. B-Environ.*, 2016, **181**, 818-824; (b) C. M. Pecoraro, M. Bellardita, V. Loddo, F. Di Franco, L. Palmisano and M. Santamaria, *J. Ind. Eng. Chem.*, 2023, **118**, 247-258.
11. A. Di Paola, M. Addamo, M. Bellardita, E. Cazzanelli and L. Palmisano, *Thin Solid Films*, 2007, **515**, 3527-3529.
12. (a) L. Mino, F. Pellegrino, S. Rades, J. Radnik, V. D. Hodoroaba, G. Spoto, V. Maurino and G. Martra, *ACS Appl. Nano Mater.*, 2018, **1**, 5355-5365; (b) M. Monai, T. Montini and P. Fornasiero, *Catalysts*, 2017, **7**, 19.
13. M. Falk, *Spectrochim. Acta Part A Mol. Spectrosc.*, 1984, **40**, 43-48.
14. (a) L. Mino, C. Negri, R. Santalucia, G. Cerrato, G. Spoto and G. Martra, *Molecules*, 2020, **25**, 4605; (b) L. Mino, A. Morales-García, S. T. Bromley and F. Illas, *Nanoscale*, 2021, **13**, 6577-6585.
15. M. Bellardita, A. Di Paola, L. Palmisano, F. Parrino, G. Buscarino and R. Amadelli, *Appl. Catal. B Environ.*, 2011, **104**, 291-299.
16. L. Mino, G. Spoto, S. Bordiga and A. Zecchina, *J. Phys. Chem. C*, 2012, **116**, 17008-17018.
17. K. I. Hadjiivanov, *J. Chem. Soc., Faraday trans.*, 1998, **94**, 1901-1904.
18. L. Lan, H. Daly, Y. Jiao, Y. Yan, C. Hardacre and X. Fan, *Int J Hydrogen Energy*, 2021, **46**, 31054-31066.
19. R. M. Navarro, J. Arenales, F. Vaquero, I. D. González and J. L. G. Fierro, *Catal Today*, 2013, **210**, 33-38.
20. M. Carosso, T. Fovanna, A. Ricchebuono, E. Vottero, M. Manzoli, S. Morandi, R. Pellegrini, A. Piovano, D. Ferri and E. Groppo, *Catal. Sci. Technolog.*, 2022, **12**, 1359-1367.
21. H. V. Thang, G. Pacchioni, L. DeRita and P. Christopher, *J. Catal.*, 2018, **367**, 104-114.

